Solar Energy Materials & Solar Cells 235 (2022) 111467

Contents lists available at ScienceDirect

Solar Energy Materials and Solar Cells

journal homepage: www.elsevier.com/locate/solmat

Reassessment of the intrinsic bulk recombination in crystalline silicon

T. Niewelt [a,b,*], B. Steinhauser [a,**], A. Richter [a,***], B. Veith-Wolf [c], A. Fell [a], B. Hammann [a], N. E. Grant [d], L. Black [e], J. Tan [f], A. Youssef [f], J.D. Murphy [d], J. Schmidt [c], M.C. Schubert [a], S. W. Glunz [a,b]

[a] Fraunhofer Institute for Solar Energy Systems ISE, Heidenhofstraße 2, 79110, Freiburg, Germany
[b] INATECH, University of Freiburg, Emmy-Noether-Straße 2, 79110, Freiburg, Germany
[c] Institute for Solar Energy Research ISFH, Am Ohrberg 1, 31860, Emmerthal, Germany
[d] School of Engineering, University of Warwick, Coventry CV4 7AL, United Kingdom
[e] School of Engineering, Building 31, The Australian National University, Canberra ACT, 2600, Australia
[f] SunPower Corporation, 51 Rio Robles, San Jose, CA, 95134, USA

ARTICLE INFO

Keywords:
Auger recombination
Charge carrier lifetime
Silicon
Single-junction maximum efficiency
Intrinsic recombination
Parameterisation

ABSTRACT

Characterisation and optimization of next-generation silicon solar cell concepts rely on an accurate knowledge of intrinsic charge carrier recombination in crystalline silicon. Reports of measured lifetimes exceeding the previous accepted parameterisation of intrinsic recombination indicate an overestimation of this recombination in certain injection regimes and hence the need for revision. In this work, twelve high-quality silicon sample sets covering a wide doping range are fabricated using state-of-the-art processing routes in order to permit an accurate assessment of intrinsic recombination based on wafer thickness variation. Special care is taken to mitigate extrinsic recombination due to bulk contamination or at the wafer surfaces. The combination of the high-quality samples with refined sample characterisation and lifetime measurements enables a much higher level of accuracy to be achieved compared to previous studies. We observe that reabsorption of luminescence photons inside the sample must be accounted for to achieve a precise description of radiative recombination. With this effect taken into account, we extract the lifetime limitation due to Auger recombination. We find that the extracted Auger recombination rate can accurately be parameterized using a physically motivated equation based on Coulomb-enhanced Auger recombination for all doping and injection conditions relevant for silicon-based photovoltaics. The improved accuracy of data description obtained with the model suggests that our new parameterisation is more consistent with the actual recombination process than previous models. Due to notable changes in Auger recombination predicted for moderate injection, we further revise the fundamental limiting power conversion efficiency for a single-junction crystalline silicon solar cell to 29.4%, which is within 0.1%$_{abs}$ compared to other recent assessments.

1. Introduction

In recent years, we have seen significant improvements in the electrical quality of industrially feasible silicon wafers. This was primarily driven by improved material growth and wafer manufacturing techniques and the development of processing steps to mitigate contamination giving rise to recombination in the silicon bulk. The ongoing rapid improvement of solar cell efficiencies in both research and mass-production is largely driven by further reduction of recombination at interfaces and surfaces via the improvement of passivation layers [1–8]. This has led to measured effective charge carrier lifetimes τ_{eff} significantly exceeding the most widely used parameterisation of the intrinsic limit of silicon by Richter et al. [9], as shown e.g. in Refs. [10,11]. Further improvements in solar cell fabrication processes and next generation solar cell concepts (e.g. TOPCon [12]/POLO [13]) will continue to exacerbate the need for an accurate description of intrinsic

* Corresponding author. INATECH, University of Freiburg, Emmy-Noether-Straße 2, 79110, Freiburg, Germany.
** Corresponding author.
*** Corresponding author.
E-mail addresses: tim.niewelt@ise.fraunhofer.de (T. Niewelt), bernd.steinhauser@ise.fraunhofer.de (B. Steinhauser), armin.richter@ise.fraunhofer.de (A. Richter).

https://doi.org/10.1016/j.solmat.2021.111467
Received 13 September 2021; Received in revised form 20 October 2021; Accepted 22 October 2021
Available online 24 November 2021

recombination in silicon. With current passivation layers allowing for carrier lifetimes exceeding the hitherto perceived theoretical limit, both characterisation of further advancements and simulation of their exploitation are limited. Therefore, we have undertaken a long-term endeavour to create an improved description of Auger recombination [9,14]. This work presents the results of the ongoing process optimization and more than three years of silicon wafer selection and preparation as well as refinement of charge carrier lifetime characterisation. Reduction of the impact of extrinsic recombination channels to a minimum was achieved via the state-of-the-art surface passivation layers and thickness variation experiments. This allows us to reassess recombination via intrinsically limiting processes of radiative and Auger recombination with a new precision.

Due to the indirect band gap of silicon, *radiative recombination* is not predominant. Since an electron and a hole are involved in the process, the total rate of radiative recombination $R_{\mathrm{rad,tot}}$ in dependence of their respective concentrations n and p reads

$$R_{\mathrm{rad,\ tot}} = B_{\mathrm{rad}}\, np \tag{1}$$

The coefficient B_{rad} in this relation includes effects of the band structure of the silicon crystal and can be determined by luminescence rate measurements (e.g. Refs. [15,16]) or derived from band-to-band absorption measurements via the generalized Planck law [17]. One important factor incorporated in B_{rad} is the effect of Coulomb interaction of the involved electron and hole – and the fact that this interaction can be screened by surrounding charge carriers [16,18]. At moderate temperatures, the transition between negligible and dominant screening occurs around the range of charge carrier densities between $10^{12}/\mathrm{cm}^3$ and $10^{18}/\mathrm{cm}^3$ and must therefore be taken into account carefully in any model intended for use in silicon photovoltaic applications [17]. This is usually done via an injection-dependent factor B_{rel} multiplied with experimentally assessed values for B_{rad} using high resistivity silicon which we denote as B_{low} [15,17,19]. In this work, we account for screening via an implementation of the random-phase approximation band gap narrowing model of Schenk [20] as motivated in a recent contribution by Fell et al. [21]. We also apply the considerations of Fell et al. to determine the fraction f_{PR} of photons emitted by radiative recombination that is reabsorbed within the sample. Since such reabsorption results in new electron hole pairs, it must be considered for precise assessment of radiative recombination.

Auger recombination describes the nonradiative recombination of an electron (e) and a hole (h) with the excess energy being transferred to a third electron or hole. Assuming the three particles to be quasi-free inside the silicon crystal, the two possible processes (referred to by the involved carriers as *eeh* or *ehh*) are considered independent and determined by the coefficients C_{eeh} and C_{ehh} and the respective carrier concentrations n and p. Then, the sum of the resulting rates represents the total rate of Auger recombination:

$$R_{\mathrm{Auger,tot}} = R_{\mathrm{eeh}} + R_{\mathrm{ehh}} = C_{\mathrm{eeh}}\, n^2 p + C_{\mathrm{ehh}}\, np^2 \tag{2}$$

However, previous works have established and demonstrated that Auger recombination processes in silicon are affected by interaction of the involved charge carriers with the crystal lattice and other free charge carriers [9,22–25] (and references therein). An important effect for charge carrier concentrations below $10^{17}/\mathrm{cm}^3$ is an enhancement of Auger recombination caused by the Coulomb interactions of the charge carriers mentioned above as addressed and demonstrated by Hangleiter and Häcker [23]. Again, for high charge carrier densities, this influence is suppressed by free-carrier screening. Therefore, Auger recombination is then well-described by the simple relation suggested in eq. (2) again. In this work, the impact of Coulomb enhancement of Auger recombination is accounted for by considering enhancement factors g_{eeh} and g_{ehh} as suggested by Hangleiter and Häcker [23] which will be discussed in section 3. The parameterisation by Richter et al. [9] included empirical terms to describe the dependence of Auger recombination on doping and injection separately. We find in retrospect that this artificial divide was only necessary due to impacts of extrinsic recombination channels on the used data set.

Any measured effective charge carrier lifetime τ_{eff} describes the net recombination rate as difference of total recombination and total generation $\Delta R = R_{\mathrm{tot}} - G_{\mathrm{tot}}$ in a given situation. Besides extrinsic carrier injection or generation this includes equilibrium generation rates. Hence the term we apply for the lifetime limitation induced by recombination path x is

$$\tau_{\mathrm{x}} := \frac{\Delta n}{\Delta R_{\mathrm{x}}} = \frac{\Delta n}{R_{\mathrm{x,tot}} - G_{\mathrm{x,0}}} \tag{3}$$

The generation term $G_{\mathrm{x,0}}$ is equal to the respective equilibrium recombination rate and hence calculated with the equilibrium carrier densities n_0 and p_0. It is numerically negligible in most application cases.

2. Experiment

Measurements to ascertain the intrinsic charge carrier lifetime τ_{intr} require both the detection and mitigation of extrinsic recombination channels and reliable charge carrier lifetime measurements. Special care was taken to select samples and process routes to reduce recombination caused by extrinsic bulk defects, as well as reducing recombination at the sample surfaces by state-of-the-art surface passivation. The experiments and sample characterisation were designed to reduce and assess uncertainties wherever possible. This includes assessment of bulk recombination via the thickness variation method [26] to take even ultra-low surface recombination into account without any extrapolation between different materials.

2.1. Sample preparation

The most accurate method to determine bulk recombination when the diffusion length is large compared to the sample thickness is to correct for surface recombination by varying the sample thickness. Assuming that a sample set based on the same bulk material and processed together (e.g. as in Ref. [27]) will possess comparable surface passivation, variation of sample thickness allows extraction of all thickness-dependent terms [26]. This approach has been applied in a limited manner in previous parameterisations of intrinsic recombination, primarily to assess surface recombination for the used dielectric layer stacks [9,14,25]. For the present study we instead make use of a large number of thickness variation sets in order to avoid the extrapolation of surface recombination between different samples of e.g. varied doping. The investigated sample sets are listed in Table 1. The method becomes more reliable given a larger thickness range, so long as consistent material parameters and surface passivation quality can be ensured for the samples used. Thus, we fabricated several sample sets featuring systematic thickness variation (i.e. sets N100, N2.3, N1.9 and P80) by purposefully cutting them from high-purity float zone silicon (FZ Si) ingots obtained directly from the crystal grower. To extend the resistivity range and data space, further sample sets were created from materials that had been found to feature excellent bulk lifetimes in earlier studies. These further sample sets were created from thermally pretreated FZ Si wafer sets either by mechanical grinding (i.e. sets N670, N80, N1.1, P80, P1.1 and P0.5) followed by mechanical and chemical surface polishing, or by prolonged wet chemical etching (i.e. sets P0.6 and P1.5). The starting wafers were chosen carefully to originate from the same box and hence likely neighbouring parts of the same original crystal.

The thermal pretreatment was found to be necessary, since although the used FZ Si is very pure and features a high crystallographic quality, it still contains defects that can cause significant extrinsic charge carrier recombination. It has been shown in the past that thermal treatments in the typical processing temperature range between 400 and 1000 °C can increase or reduce this unwanted recombination activity [28,29]. The

Table 1
Thickness variation sample sets (all cut from FZ Si ingots).

Set	Dopant[a]	Resistivity at R.T. [Ωcm]	Samples[b] (used/ processed)	Thickness range[b] [μm]	Passivation[c]
N1.1	P	1.09	7/12	93–425	TOPCon
N1.9	P	1.88	3/6	137–1414	TOPCon
N2.3	P	2.27	8/9	140–1437	TOPCon
N100	P	~100	2/5	100–1500	TOPCon
N80	P	~80	4/11	94–314	TOPCon
N670	P	~670	4/9	93–480	TOPCon
P0.6	B	0.6	4/12	83–272	Al_2O_3
P0.5	B	0.5	4/12	230–506	Al_2O_3
P1.5	B	1.5	6/12	82–273	Al_2O_3
P1.1	B	1.09	5/14	96–546	TOPCon
P3.0	B	3.01	5/9	100–1500	TOPCon
P80	B	~80	3/12	93–290	TOPCon

[a] P: phosphorus, B: boron.
[b] a larger sample set was processed and only samples with excellent passivation were picked for the final evaluation. The given thickness range refers to the used samples.
[c] see Appendix A section for processing details.

occurrence of these defects is usually indicated by a characteristic pattern of lateral lifetime non-uniformity where the central area of the wafers is more affected. The defect occurrence can be avoided by the application of high process temperatures [28,30]. In a reassessment of the sample set used by Richter et al. for the previous parameterisation [9], we observed that some of the wafers showed a faint defect signature when characterised by photoluminescence imaging (PLI), indicating an extrinsic limitation. To avoid this detrimental impact on the new parameterisation, the wafers in this study underwent a specific process route including a thermal oxidation and external gettering step developed in a previous work of the author consortium [10]. All fabricated samples were passivated with state-of-the-art surface passivation layers via specifically optimized process routes. The used TOPCon layer stacks were optimized for optimum surface passivation as discussed in Ref. [27]. The aluminium oxide layers were deposited via plasma-assisted atomic layer deposition (PA-ALD) in a FlexAL™ reactor, as discussed in Ref. [14]. For a more detailed overview on the applied processes the reader is referred to the Appendix section A where Fig. 5 shows a flow chart of the processing routes.

Besides the specifically processed sample sets, additional passivated wafers were provided by an industry partner. These wafers from Czochralski-grown n-type silicon wafers cover the resistivity range of 1.4 to 0.18 Ωcm and were especially useful to extend the n-type doping range to concentrations above 10^{16} cm^{-3}. The samples were all of similar thickness and hence the direct extraction of bulk lifetimes was not possible.

2.2. Sample overview

Table 1 holds an overview on the sample sets processed for this work. More information on the sample processing – including a process flow sketch – is included in the Appendix section A.

2.3. Lifetime measurement

Most wafers were subjected to spatially resolved photoluminescence imaging characterisation in a *modulum* tool [31] to identify the region on the sample least affected by local flaws in surface passivation or handling damage. This imaging setup allows for in situ lifetime calibration of PLI and hence diffusion length assessment, which was helpful to identify samples not suitable for further analysis due to extrinsic effects such as sample handling induced damage.

The characterisation of the total recombination R_{tot} as a function of Δn in each sample was performed by photoconductance decay (PCD) measurements using Sinton Instruments WCT-120 lifetime testers carefully calibrated to account for sample thickness [32] (see also calibration data in the Appendix C). Both measurement modes – i.e. with short and long flashes were recorded for all samples. The available injection level range of the gathered charge carrier lifetime curves $\tau_{eff}(\Delta n)$ was increased by changing integration times and flash distance and subsequently stitching multiple measurements. To ensure validity of the measured lifetimes they were cross-checked with self-consistent measurement methods based on modulated photoluminescence measurements [31,33].

2.4. Lifetime data evaluation

Multiple lifetime measurements were performed for each sample with varied measurement parameters. Besides self-consistent transient PCD measurements we also performed measurements featuring a slow-decaying flash. Due to the high quality and lateral homogeneity of the samples it was possible to assess the optical factors f_{opt} necessary for the generalized evaluation of such measurements from direct comparison to transient lifetime data. The determined values for f_{opt} were consistent on most sample sets. When unexpected variations in the optical factor of more than 0.05 were observed, the respective measurements were given less weighting in the final fit to the data. As discussed in the recent contribution by Black and Macdonald [34] the common approach of PCD measurement evaluation provided by the current Sinton Lifetime tester software is not precise in certain charge carrier concentration regimes. Following the suggestions in Ref. [34] we therefore evaluated the raw data with our own purpose-built software, which makes use of the Klaassen mobility model [35,36] to determine the time-dependent excess charge carrier density $\Delta n(t)$ from the measured total sample conductance $\sigma(t)$. A 2-point centralized derivative was used for assessment of the transient terms of carrier decay [37]. Measurement noise and electronic artefacts were removed as outlined in the Appendix (Section C).

2.4.1. Measured effective charge carrier lifetimes

The thickness variation experiments performed for this work were found to feature excellent effective charge carrier lifetimes τ_{eff}, as anticipated based on the application of the optimized process. In the investigated resistivity range the achievable τ_{eff} are very sensitive to surface recombination. Our sample preparation was designed to create optimal surface passivation, but due to the variation in sample dimensions, manual sample handling cannot be avoided completely. We found that even slight imperfections outside the measurement area affected the evaluation due to the long diffusion lengths in the studied samples and the additional lateral conductivity induced by the passivation layers, c.f. [38]. As a consequence, some samples were discarded from the evaluation based on the PLI results and the used samples represent only a fraction of the originally processed samples (c.f. also Table 1). Lifetime measurements on the remaining samples were refined as discussed below and in Appendix Section C. Fig. 1 shows example lifetime curve sets for two of the investigated sample sets. The lifetimes measured in this study are among the highest measured lifetimes in silicon samples of the respective doping. The effective lifetimes measured on the samples of set N670 reach 0.5 s and are the highest lifetimes ever reported for silicon to date [33]. A comparison of the highest τ_{eff} measured in this study to previously reported lifetimes and the Richter et al. parameterisation is shown in the Appendix (Fig. 8).

2.4.2. Extraction of bulk lifetime

In order to assess intrinsic limitation, we need to distinguish the recombination channels that are incorporated within the measured τ_{eff} curves. Recombination at the interface between silicon and the passivation layer can be corrected for by evaluating the lifetime dependence on the silicon wafer thickness W via

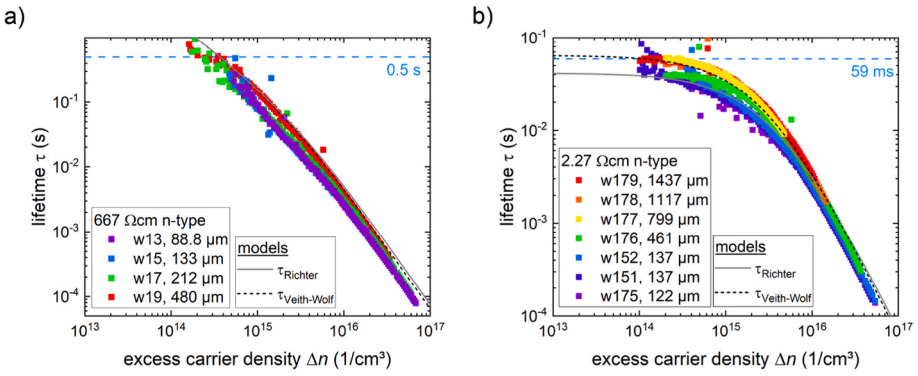

Fig. 1. Measured lifetimes and extracted lifetimes for the thickness variation sample sets N670 (a) and N2.3 (b). The dashed horizontal lines illustrate the highest measured τ_{eff} used to include the measurements in the record lifetime comparison graph in Fig. 8 in the Appendix. The surface recombination velocity extracted from the measurement series is shown in Fig. 9 in the Appendix.

$$\tau_{eff}(W) = \left(\frac{1}{\tau_{bulk}} + \frac{1}{\tau_{surface}(W)}\right)^{-1} = \left(\frac{1}{\tau_{bulk}} + \frac{2R_{surface}}{W}\right)^{-1} \quad (4)$$

$$\tau_{bulk} = \lim_{W\to\infty}\left(\tau_{eff}(W)\right) \quad (5)$$

This evaluation assumes τ_{bulk} and recombination at the wafer surfaces $R_{surface}$ to be the same for all samples of one set. Then, a linear relation is expected between $(\tau_{eff})^{-1}$ and $1/W$ and the extrapolation to $1/W = 0$ (i.e. W≈∞) can be used to extract τ_{bulk}. The linearity can also help to assess the validity of extracted bulk lifetimes. Our processing routes were designed to reduce extrinsic bulk recombination to a minimum and otherwise ensure that potential remaining limitations would be comparable in the samples of each set. However, direct extraction of τ_{bulk} from τ_{eff} with eq. (5) would just be an approximation because there is a difference in the impact of radiative recombination between the samples. As suggested by Kerr et al. [39] and discussed further by Fell et al. [21], the reabsorption of radiatively emitted photons inside the sample cannot be assumed independent of sample thickness and surface condition. For planar samples the significant total internal reflection of many photons means that >80% of photons are reabsorbed within the sample itself. Reabsorption can occur via intra-band absorption of free carriers, referred to as free carrier absorption (FCA), or via band-to-band absorption. The latter effect is termed photon recycling (PR) and creates free electron-hole pairs with rate G_{PR}. Since G_{PR} is directly linked to the rate $R_{rad,tot}$ it can be accounted for by a term (1-f_{PR}) to be

$$R_{rad,\,eff} = R_{rad,tot}\cdot(1 - f_{PR}) = B_{low}B_{rel\,(n,p)}\left(1 - f_{PR\,(n,p,sample)}\right) np \quad (6)$$

The fraction f_{PR} of reabsorbed photons in every sample was assessed via the analytical model described in Ref. [21] taking FCA into account. Appendix section F contains a polynomial approximation for f_{PR} of typical sample structures. It should be noted that FCA and PR are competing processes and therefore precise modelling of radiative recombination in highly injected silicon should take FCA into account to accurately assess f_{PR}.

We subtract $R_{rad,eff}$ from each $R_{eff} = 1/\tau_{eff}(\Delta n)$ curve prior to the evaluation of the thickness-dependent sample sets. Thus, we can directly isolate τ_{Auger} which is the dominant intrinsic recombination source in silicon under most circumstances. For this purpose, we applied the low-carrier-density-limit of the radiative recombination coefficient B_{low} of 4.76×10^{-15} cm^{-6} determined by Nguyen et al. [15] multiplied by B_{rel} calculated via the band gap narrowing model of Schenk [20] to account for Coulomb screening, as introduced in Ref. [21].

The resulting extracted $\tau_{Auger}(\Delta n)$ for the twelve thickness-dependent sample sets are shown in Fig. 2a. Excellent lifetime levels at low charge carrier densities are observed, and the lifetimes are comparable to or above previously reported record lifetimes. The direct comparison of the curves shows all curves tend to converge at high injection densities. This illustrates an improved consistency of measurement data quality compared to Ref. [9], since τ_{Auger} of highly-injected silicon is expected to coincide for p- and n-type doping.

An extraction of τ_{Auger} with the approach described above was not possible for the additional n-type samples of high doping concentration due to the single wafer thickness. Therefore, the τ_{eff} were corrected for radiative recombination and a reasonable surface recombination of 0.5 fA/cm^3. This assumption results in a lower reliability of τ_{Auger} and was accounted for by a reduced weight in the subsequent fit.

3. Parameterisation of intrinsic recombination

For the description of the lifetime limitation via Auger recombination we apply

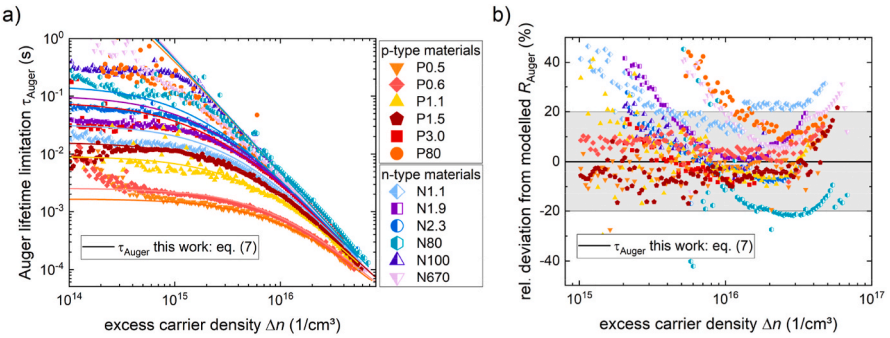

Fig. 2. a) Extracted Auger lifetime limitations τ_{Auger} for the investigated thickness-dependent sample sets. The lines indicate the parameterisation of Auger recombination suggested in this work as evaluated with eq. (7) and the parameters given in Table 2 b) Relative deviation of the experimentally extracted R_{Auger} from the suggested model with the grey area indicating 20% deviation. The plot shows the part of the original data that was used for the final fit.

$$\tau_{\mathrm{Auger}} := \frac{\Delta n}{C_{\mathrm{eeh}} g_{\mathrm{eeh}}(n^2 p - n_0^2 p_0) + C_{\mathrm{ehh}} g_{\mathrm{ehh}}(np^2 - n_0 p_0^2)} = \frac{\Delta n}{\Delta R_{\mathrm{Auger}}} \tag{7}$$

A parallel publication by Black and Macdonald [34] reviews literature data on Auger recombination in highly-doped silicon. It is discussed that the commonly used Auger coefficients C_{eeh} and C_{ehh} by Dziewior and Schmid [40] need to be corrected using up-to-date mobility models. To achieve a good description of the corrected data, Black and Macdonald suggest values of $C_{\mathrm{eeh}} = 3.41 \times 10^{-31}$ cm^{-6}s^{-1} and $C_{\mathrm{ehh}} = 1.17 \times 10^{-31}$ cm^{-6}s^{-1}. We adapt these values for our parameterisation, because this work does not report new data points for the high doping concentrations, where C_{eeh} and C_{ehh} can best be determined.

The terms g_{eeh} and g_{ehh} were introduced to reflect Coulomb enhancement due to the interactions of unscreened charge carriers. They are functions of charge carrier density and describe the transition between pronounced Coulomb enhancement for low carrier concentrations to its absence at higher concentrations. There is no simple analytical expression for the effect of the three-particle interaction [23]. Therefore we investigated the different approaches chosen in previous works, e.g. Refs. [9,22,24,34,41]. In analogy to the work of Black and Macdonald we chose to adapt the empirical formalism suggested by Jonsson et al. [41] which we restructured and changed to account for the sum of both carrier concentrations to provide a more coherent behaviour for highly-injected silicon [25]. The expression for g_{exh} we used to describe our data is

$$g_{\mathrm{exh}} = 1 + (g_{\mathrm{exh,max}} - 1)\frac{1}{1 + \left(\frac{n+p}{N_{\mathrm{ref}}}\right)^{\alpha_{\mathrm{Auger}}}} \tag{8}$$

with 'x' standing for e and h, as appropriate. We adopt the empirical exponent $\alpha_{\mathrm{Auger}} = 2$ used by Jonsson et al. since it appears to provide a good description of the transition region. We tested different values for the Mott transition density N_{ref} and found good agreement with literature data and our data for a value of 4×10^{17} cm^{-3}. Above values of ~3×10^{17} cm^{-3} the choice of N_{ref} mostly impacts description of literature data whose quality we do not reassess and therefore our choice is mainly motivated to achieve consistency with literature data and the previous parameterisation of Richter. The two Coulomb-enhancement magnitude factors $g_{\mathrm{exh,max}}$ were consequently used as the only free fit parameters in our Auger model. Our fitting routine indicates that reasonable fits can be achieved with the assumption of equal factors $g_{\mathrm{eeh,max}} = g_{\mathrm{ehh,max}}$. While the implication of identical screening behaviour for both capture processes is interesting, we decided to exploit the additional degree of freedom for an improved fit quality, and find an improved accuracy with values of $g_{\mathrm{eeh,max}} = 4.38$ and $g_{\mathrm{ehh,max}} = 4.88$. It should be noted that this implies Coulomb enhancement for low injection significantly smaller than suggested in literature [23,24]. The final parameterisation is in good agreement with the one suggested by Black and Macdonald [34]. An especially good agreement is observed when it comes to the ambipolar Auger coefficient they determined at injection densities of pronounced Coulomb-enhancement $C_{\mathrm{amb,CE}} = C_{\mathrm{eeh}} g_{\mathrm{eeh}} + C_{\mathrm{ehh}} g_{\mathrm{ehh}}$ to be 2.11×10^{-30} cm^{6}s^{-1} – which is within 2% of our finding. Fig. 2 illustrates the description of the $\tau_{\mathrm{Auger}}(\Delta n)$ data set extracted from thickness-dependent measurements.

The combination of this improved description of Auger recombination with a consistent description of radiative recombination allows for more precise modelling of the intrinsic lifetime limitation in silicon.

$$\tau_{\mathrm{intr}} := \frac{\Delta n}{\Delta R_{\mathrm{intr}}} = \frac{\Delta n}{\Delta R_{\mathrm{Auger}} + \Delta R_{\mathrm{rad}}} \tag{9}$$

Due to the effect of PR on radiative recombination, this theoretical intrinsic lifetime cannot directly be observed with most measurement methods. For the description of experimentally assessable charge carrier lifetime we suggest using the term

$$\tau_{\mathrm{intr,exp}} = \frac{\Delta n}{(np)(C_{\mathrm{eeh}} \cdot g_{\mathrm{eeh}} \cdot n + C_{\mathrm{ehh}} \cdot g_{\mathrm{ehh}} \cdot p + B_{\mathrm{low}} \cdot B_{\mathrm{rel}} \cdot (1 - f_{PR}))} \tag{10}$$

in conjunction with eq. (8) and the information from Table 2. The graphs in Fig. 3 compare the model to the highest reported charge carrier lifetimes in silicon from this work, our previous work [10], and literature.

The given model is valid for a sample temperature of 300 K. Many applications of the model will likely not require accurate knowledge of f_{PR} because radiative recombination plays a minor role compared to extrinsic and Auger recombination. Thus, a precise value of f_{PR} will be of minor importance in many assessments of effective carrier lifetimes. For convenience, simple polynomial estimations of f_{PR} for two common cases – mirror-like reflection at planar surfaces and diffuse scattering at textured surfaces – are given in appendix section F. Notably, for the case of mirror-like planar surfaces, f_{PR} is very high (i.e. about 0.9 with little dependence on sample thickness). This means that neglecting radiative recombination entirely (i.e. assuming $f_{\mathrm{PR}} = 1$, thus $\tau_{\mathrm{intr,exp}} \approx \tau_{\mathrm{Auger}}$) in such samples may be a better assumption than not considering PR. For more detailed discussion of the relevance of reabsorption and an approach to determine it for given samples the reader is referred to Ref. [21].

A discussion of the measurement uncertainties of the used data is included in the appendix. The impact of uncertainty of parameters like sample resistivity and thickness as well as potential lateral inhomogeneity on the lifetime data – and hence the parameterisation – could not fully be assessed. The reader is referred to Fig. 2b) which demonstrates that the extracted R_{Auger} data of all materials agree well with a confidence interval of ±20% to modelling using the suggested parameters (given in Table 2).

3.1. Impact on derived parameters

It should be kept in mind that since the new model predicts different recombination rates than previous ones this implies a change in derived parameters such as surface recombination saturation currents J_0. Where the new parameterisation predicts higher τ_{bulk} – for example around 1 Ωcm n-type – an evaluation of the same measured τ_{eff} will yield higher J_0 and vice versa. The new parameterisation also predicts significantly different intrinsic recombination compared to Ref. [9] for highly-doped silicon, as shown in Fig. 9 in Appendix section E. This change is caused by the revision of literature data suggested by Black and Macdonald [34] and the resulting C_{eeh} and C_{ehh}, as well as the different form of the parameterisation formula. The changed behaviour significantly impacts the simulation of J_0 for highly-doped surfaces for which the contribution of Auger recombination is often substantial. Particular care needs to be taken when using existing parameterizations of surface recombination velocities from literature, e.g. Refs. [47,48], or the band-gap narrowing model by Yan and Cuevas [49] within such simulations, as those parameterizations have been derived from experiments using [9].

Table 2
Recommended parameters and models to describe the intrinsic charge carrier lifetime limitation of a given sample with eqs. (10) and (8).

Parameter	Value/Model	Reference
C_{eeh}	3.41×10^{-31} cm^{6}s^{-1}	[34]
C_{ehh}	1.17×10^{-31} cm^{6}s^{-1}	[34]
g_{eeh}	eq. (8) with $g_{\mathrm{eeh,max}} = 4.38$	This work
g_{ehh}	eq. (8) with $g_{\mathrm{ehh,max}} = 4.88$	This work
N_{ref}	4×10^{17} cm^{-3} (for use in eq. (8))	This work
α_{Auger}	2 (for use in eq. (8))	[41]/This work
B_{low}	4.76×10^{-15} cm^{3}s^{-1}	[15]
B_{rel}	Model of Coulomb enhancement	[17]/[20,21]
f_{PR}	Optical model of given sample/cell	[21]/Appendix of this work

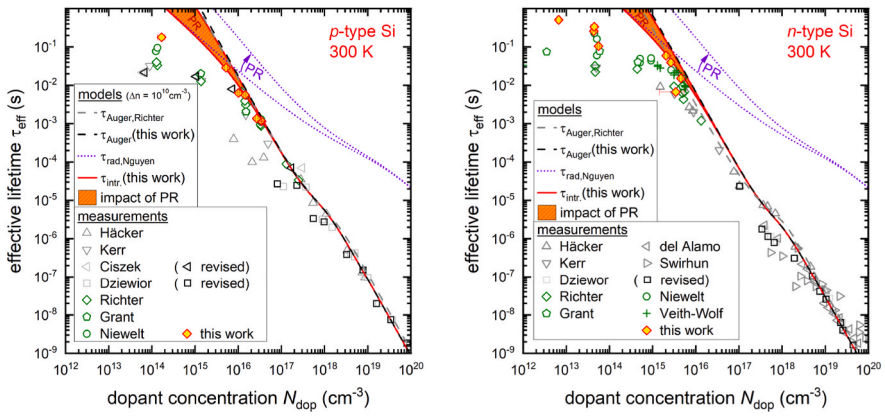

Fig. 3. Illustration of the suggested model for τ_{Auger} and the importance of photon recycling on the intrinsic lifetime limitation in lowly-injected p-type (left) and n-type (right) silicon. Literature data for measured effective lifetimes is shown for comparison [9,10,14,22,39,40,42–46]. A zoom to the region of low doping concentrations is shown in Fig. 8 in the Appendix. (For interpretation of the references to colour in this figure legend, the reader is referred to the Web version of this article.)

4. Reassesment of the theoretical limit of silicon solar cell efficiency

The improved model for intrinsic recombination leads to a change in the theoretical limit for the power conversion efficiency of single-junction crystalline silicon solar cells, which is therefore reassessed in this section. The limit was reassessed in a work by Schäfer and Brendel [50], which adjusted the calculations by Richter et al. [51] to improve the description of Lambertian light-trapping, resulting in an efficiency limit of 29.57%. More recently, an updated Auger parameterisation for n-type material was used in the same modelling approach, resulting in an efficiency limit of 29.47% [14]. For the ideal efficiency simulations in this work we use the solar cell simulation software Quokka3 [52], which employs up-to-date material models for intrinsic carrier density and carrier mobility, as well as the light-trapping and photon-recycling model described in Ref. [21]. Compared to Refs. [14,50,51], Quokka3 uses more recent models for the optical properties of silicon, namely [53] for the band-to-band absorption coefficient, and [54] for FCA. Furthermore, the 1D simulations include transport losses in the silicon bulk. As of writing this manuscript, Quokka3 does not account for FCA of excess charge carriers. We find that all these individual model deviations have only a marginal impact on the calculated efficiency: a close match with ~0.01%$_{abs}$ difference between our simulations and the results of [50] is found when using the Richter model for the intrinsic lifetime. This also indicates that the light-trapping and photon recycling model implemented in Quokka3 are equivalent to the accurate Lambertian limit in Ref. [50].

The maximum efficiency is obtained for undoped silicon with a thickness of ~100 µm, for which the carrier density at maximum power point is ~6×10^{15} cm^{-3}. At this injection level the improved Auger model of this work predicts a significantly higher recombination compared to Richter [9] resulting in a slight reduction of the efficiency limit to 29.4% (V_{oc} = 757 mV, J_{SC} = 43.4 mA/cm^2, FF = 89.5%). Notably, despite several differences in model assumptions, all recent publications on efficiency limits deviate only insignificantly in the range from 29.4% to 29.6%.

In Fig. 4 the limiting efficiency for undoped, as well as 1 Ωcm n-type and p-type material are plotted as a function of cell thickness, comparing Richter's [9] and this work's parameterisation. It can be seen that the impact of doping on the efficiency limit has become significantly less with this work's reassesment of Auger recombination.

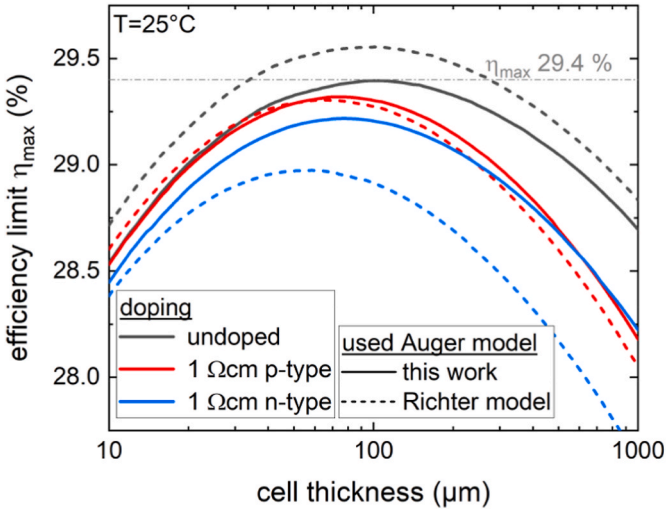

Fig. 4. Theoretical limit of solar cell efficiency η_{max} according to simulation with Quokka3. Solid lines were calculated with the Auger model presented in this work in comparison to the Richter model [9] depicted in dashed lines.

5. Conclusion

We have presented our work to improve the knowledge on, and description of intrinsic recombination processes in silicon samples of moderate doping and injection as relevant for solar cells. A large set of carefully chosen samples has been processed with state-of-the-art process routes to minimize the impact of extrinsic recombination. Effective charge carrier lifetimes were measured by photoconductance decay measurements. This resulted in record lifetimes of up to 0.5 s as reported in Ref. [33]. The impact of surface recombination was removed by employing the thickness variation method to extract the bulk lifetime. Radiative recombination was assessed with the parameters of Nguyen et al. [15] and the effects of photon recycling and Coulomb enhancement taken into account via optical modelling of the samples according to the suggestions by Fell et al. [21]. We find that a precise assessment of the intrinsic lifetime limit requires assessment of photon recycling effects and hence depends on the specific sample morphology. A simple polynomial estimation is given in the appendix of the paper but for a more precise description we refer to Fell et al. [21].

The remaining recombination was assessed in terms of Coulomb-enhanced Auger recombination as suggested by Hangleiter and Häcker [23]. We observe that our data are in good agreement with a simple expression for Auger recombination. The effect of charge carrier screening was taken into account via a term suggested by Jonsson et al. [41] modified to account for the carrier concentration sum. With this

adjustment, Coulomb enhancement for electrons and holes can be described by the same physical model and appears to be less pronounced than anticipated in literature. For highly doped or highly injected silicon, we based our model on recently reassessed literature data and the considerations proposed by Black and Macdonald [34]. The resulting model for Coulomb-enhanced Auger limitation is thus based on a description of the fundamental recombination process.

In conjunction with recent considerations on radiative recombination, the updated intrinsic lifetime model will improve the accuracy of simulating high-efficiency solar cells and the investigation of high purity silicon materials and state-of-the art surface passivation layers. We applied the new model and found that the limiting efficiency of ideal single-junction crystalline silicon solar cells is 29.4%, which deviates only slightly from other recent assessments.

CRediT authorship contribution statement

T. Niewelt: Conceptualization, Investigation, Formal analysis, Data curation, Writing – review & editing, Writing – original draft, Visualization, Methodology, Resources. **B. Steinhauser:** Conceptualization, Data curation, Formal analysis, Investigation, Methodology, Resources, Software, Validation, Visualization, Writing – original draft, Writing – review & editing. **A. Richter:** Validation, Visualization, Writing – review & editing, Resources, Methodology, Investigation, Data curation, Conceptualization. **B. Veith-Wolf:** Investigation, Data curation, Methodology, Resources, Writing – review & editing, Conceptualization. **A. Fell:** Validation, Formal analysis, Writing – review & editing, Software, Resources, Methodology, Data curation. **B. Hammann:** Data curation, Writing – review & editing, Methodology, Investigation. **N.E. Grant:** Writing – review & editing, Resources, Methodology, Conceptualization. **L. Black:** Methodology, Resources, Writing – review & editing. **J. Tan:** Resources. **A. Youssef:** Resources. **J.D. Murphy:** Writing – review & editing, Funding acquisition, Conceptualization. **J. Schmidt:** Funding acquisition, Project administration, Writing – review & editing. **M.C. Schubert:** Conceptualization, Writing – review & editing, Supervision, Project administration, Funding acquisition. **S.W. Glunz:** Conceptualization, Funding acquisition, Project administration, Supervision, Writing – review & editing.

Declaration of competing interest

The authors declare that they have no known competing financial interests or personal relationships that could have appeared to influence the work reported in this paper.

Acknowledgement

The authors would like to thank J. Stenzenberger and A. Lenz of Wacker Chemie AG for providing some of the high purity FZ Si wafers used in this study. The fruitful discussions with R.S. Bonilla of Oxford University during the conceptualization phase of this work are highly appreciated. Sample processing and characterisation at Fraunhofer ISE was kindly supported by A. Leimenstoll, F. Schätzle, R. Neubauer and P. Vieira-Rodrigues.

This work was funded by the German Federal Ministry for Economic Affairs and Energy (BMWi) in project LIMES under the contract numbers 0324204 A (University of Freiburg), 0324204C (Fraunhofer ISE) and 0324204D (ISFH).

Work at the University of Warwick was supported by the Engineering and Physical Sciences Research Council (EP/M024911/1) and the Leverhulme Trust (RPG-2020-377).

Work at the Australian National University was supported by the Australian Renewable Energy Agency (ARENA) through project RND017.

APPENDIX

A. Sample Processing

An overview of the processing schemes can be found in Fig. 5. The processes whose thermal budget can be expected to have the most relevant impact on material quality are the oxidation and phosphorus diffusion gettering processes at and above 850 °C. Each of the processes featured 60 min at the stated temperature followed by cooldown in the furnace to temperatures around 600 °C. The processes used for TOPCon passivation are described in more detail in Ref. [27]. The deposition of aluminium oxide via PA-ALD was performed in a OpAL™ reactor for the "TOPCon" groups and in a FlexAL™ reactor for the "AlOx" group. More details on the latter process can be found in Ref. [14]. The passivation layers were fully activated via annealing at 425 °C in forming gas or a nitrogen atmosphere for 25 min.

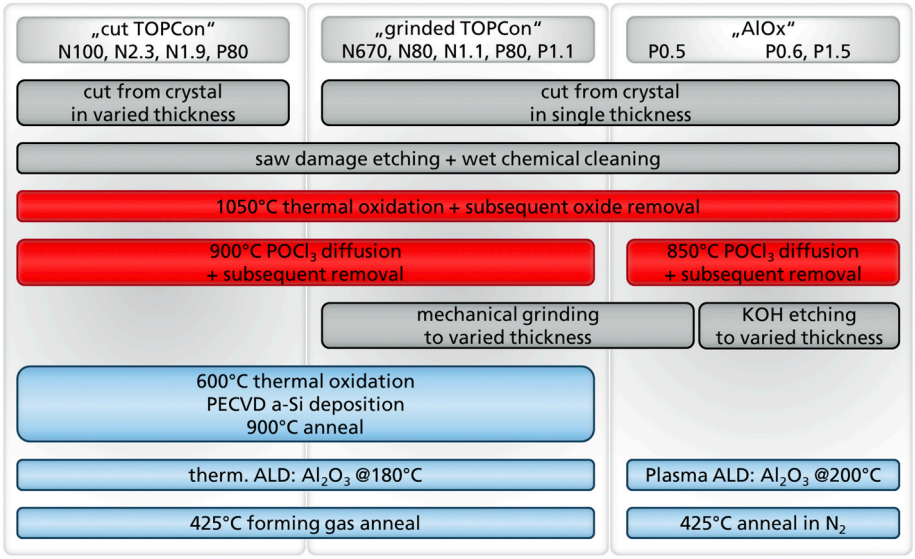

Fig. 5. Process flows of the different sample sets. Grey fields indicate the processes to define sample thickness, red fields indicate thermal pre-treatments to dissolve grown-in defects [10,28,29,55], blue fields indicate processes to passivate the sample surfaces, as discussed in Refs. [14,27].

B. Sample Characterisation

The sample thickness was determined on the lifetime samples via a photogrammetric approach allowing for good precision even on samples with irregular shapes (e.g. broken-off edges). The weight of each sample was measured using precision lab scales and the wafer area taken from wafer specification or determined using scale-calibrated photographs taken with a *modulum* PLI setup. With the camera mounted perpendicular over the samples we estimate that the area determination using a threshold-based image analysis results in less than 2% area uncertainty. The approach provides the average thickness of the whole sample, which may differ from the spots analysed in later measurements. Thickness gauge measurements of the sample thickness were used as a consistency check. Sample sets N670, N80, N1.1, P80, P1.1 and P0.5 were created via mechanical grinding using a commercial service which should provide parallel wafer surfaces or negligible angles. Sample sets N100, N2.3, N1.9 and P3.0 were created in an industrial wire-cutting setup where individual wire slots were left out to create thicker samples. A statistical analysis of inline thickness measurements in a MeyerBurger HE-WIS-06 wafer inspection tool on >750 standard wafers cut alongside set P3.0 observed average total thickness variations of 7.1 µm. Wire cutting usually creates wedge-shaped inhomogeneity thus we assume the thickness variation across the ~3 cm in diameter lifetime measurement spot to amount to 1.8 µm. Sample sets P0.6 and P1.5 were created by prolonged etching in KOH. This process can give rise to lateral inhomogeneity due to bath convection. Therefore, the thickness of the resulting samples was also analysed locally by using a thickness gauge.

The sample doping was determined from wafer resistivity measurements performed at different stages and locations on the wafers. The resistivity measurement of the Sinton Instruments Lifetime Tester during lifetime characterisation itself is influenced by the presence of the used passivation layers. Conductive layers such as the TOPCon stack or band bending caused by fixed charges within the Al_2O_3 can affect the total resistivity especially for thin samples of low resistivity bulk material. Similar to the extraction of bulk lifetimes it was found feasible to determine bulk resistivity of moderately-doped materials by evaluation of the sheet conductance change with sample thickness. Otherwise, selected samples were etched back to silicon after lifetime characterisation to allow for bulk resistivity measurements with the inductive coil, four-point-probe measurements and electrochemical capacitance-voltage (ECV) profiling.

C. Lifetime Measurements

The WCT-120 lifetime tester used for most charge carrier lifetime measurements in this work was calibrated using a large set of wafers with different thickness and resistivity. Stacks of these wafers with different permutation were used to cover a wide range of measured voltages, as shown in Fig. 6. The calibration parameters were determined following the formalism given in Ref. [32] to calculate the apparent sheet conductance $S_{\square}$ of each wafer stack using the Sinton Lifetime tester calibration software version 5.1.

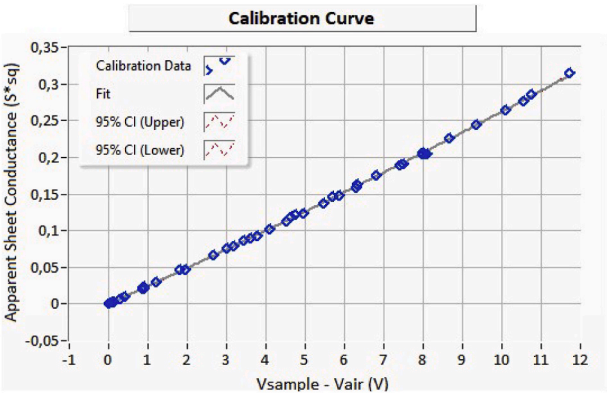

Fig. 6. Calibration data for the Sinton lifetime tester on which most data have been measured.

Table 3
Calibration parameters resulting from the measurements shown in Fig. 6

	A $S_{\square}/V^2$	B $S_{\square}/V$	Offset V	λ (mm)
Value	2.04×10^{-4}	2.418×10^{-2}	1.103×10^{-2}	4.308
Uncertainty	1.08×10^{-4}	6.11×10^{-4}	1.12×10^{-4}	0.231

Individual lifetime measurement curves were found to be affected by various types of artefacts. Some of these occur randomly and then affect a subset of data points from the measurement. Others such as oversaturation of the measurement signal for thick samples upon strong carrier injection occurred systematically. Furthermore, a slight impact of measurement signal noise was observed. The impact of noise is most pronounced in the low carrier concentration part of the curve, where weak signals are measured, and hence small signal artefacts have a strong impact. The $\tau_{eff}(\Delta n)$ curves resulting from repeated measurements were combined as follows: injection ranges exhibiting visible scatter, oscillations, jumps or kinks were discarded; subsequently, the 5–20 curves measured per sample were plotted together and curve parts were discarded when they significantly deviated from the overall trend; when the lifetime exhibited a clear maximum, the curves were only evaluated for excess carrier densities exceeding this maximum. The resulting set of partial measurement curves was interpolated and smoothed using a monotone piecewise cubic algorithm [56]. The interpolation step serves to account for fluctuations between the measurements and simplifies the subsequent comparative evaluation for the extraction of τ_{bulk} from the thickness variation. Fig. 7 illustrates the data selection process and the extracted curves on a sample from set P80. It also shows the impact of reevaluating the raw data using a custom script with improved mobility model and differentiation algorithm.

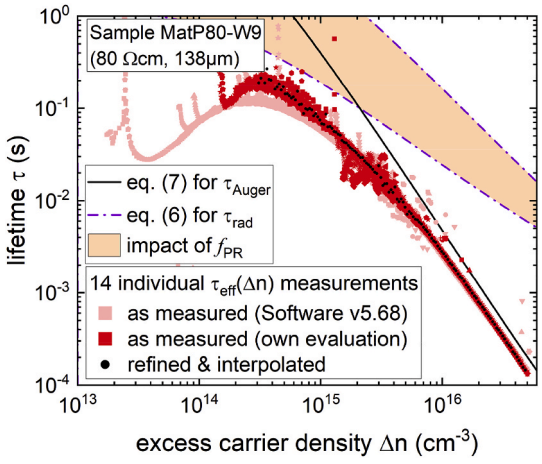

Fig. 7. Example for the data selection of the measured τ_{eff} curves on a sample from set P80.

To again illustrate the necessity of the given reparameterization of intrinsic recombination, Fig. 8 shows a direct comparison of measured lifetimes τ_{eff} from this study and earlier works to the Richter parameterisation [9].

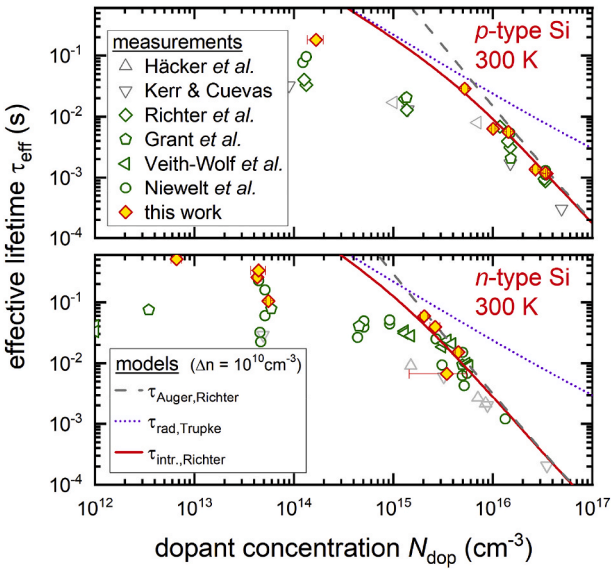

Fig. 8. Collection of highest measured effective lifetimes on p- and n-type doped samples [9,10,14,22,42,43]. The measured τ_{eff} were determined at different injection conditions. The lines were calculated with the Richter model and hence illustrate the necessity for an updated parameterisation of intrinsic recombination.

D. Bulk lifetime extraction assessment

As given in eq. (5) the evaluation of the thickness variation allows for extraction of bulk lifetime from the x-axis intercept of plotting recombination rate vs. inverse thickness. Evaluation of the slope yields the surface recombination velocity S_{eff} for the sample set at every analysed injection density. Since it is a better quantity to compare surface recombination on differently doped samples, we analysed the $S_{eff}(\Delta n)$ curves in terms of a surface recombination current $J_{0,s}$. It was fitted to the injection density range 5×10^{14}–5×10^{15} cm^{-3} using

$$S_{eff} = \frac{J_{0,s}\left(N_{dop} + \Delta n\right)}{q \cdot n_{i,0}^2} \tag{11}$$

with the elementary charge q and $n_{i,0}$ being the effective intrinsic carrier density in dark equilibrium. We did not use the resulting J_{0s} in our subsequent evaluation but it serves as quality control of the used passivation layers and sanity check for our data refinement. As expected, the used surface passivation schemes feature low surface recombination current densities around 1 fA/cm^2. It should be noted here that a quantitative comparison to literature data may be distorted as most values in literature were extracted from single samples using the method of Kane and Swanson [57] and necessarily have applied corrections for intrinsic recombination outdated by this work. Example curves for the description of the injection dependence of surface recombination are shown in Fig. 9. The deviation of $S_{eff}(\Delta n)$ from the theoretical curve was considered to decide which part of the data was fitted.

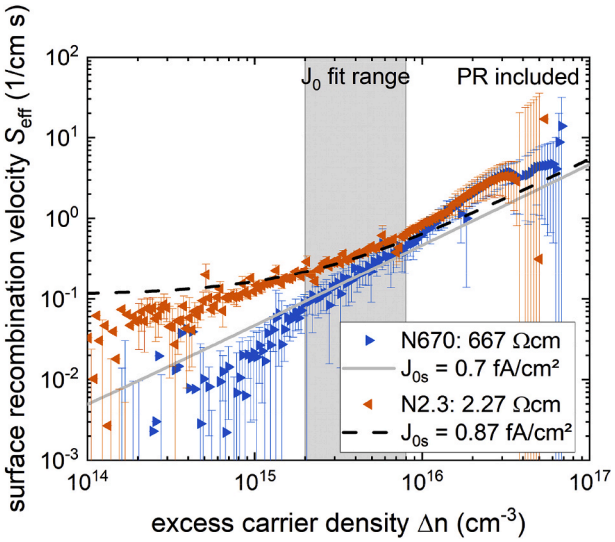

Fig. 9. Evaluation of surface recombination for the sample sets shown in Fig. 1. The indicated J_{0s} curve was calculated according to eq. (11) and serves as supporting evidence that I) most surface recombination is effectively suppressed by the used surface passivation and II) the thickness dependent evaluation gave plausible results. The J_{0s} values were not used for our further evaluation.

E. Fit assessment

The parameterisation of Auger processes suggested in this work was fitted to refined measurement data and is thus highly impacted by measurement uncertainty and systematic errors.

The uncertainty of lifetime assumed during fitting was largely based on reproducibility errors during τ_{bulk} extraction from the thickness variation experiments. The nominal uncertainty of PCD lifetime measurements with the Sinton lifetime tester has been given as ±11% for transient and ±8% for quasi-steady-state evaluation [58]. That was based on an inter laboratory round robin experiment and a smaller intra laboratory standard deviation was observed. The study focused on the comparison of fixed-injection lifetimes but also reported derived J_0 values that indicated potential additional errors for injection dependent lifetimes. Since the round robin study [58] and the more fundamental investigation by McIntosh and Sinton [59] were performed prior to crucial measurement protocol updates (e.g. Ref. [32]) we do not consider them directly applicable to assess the uncertainty of our data and hence the derived parameterisation. The complex impact of uncertainty of sample resistivity and thickness as well as potential lateral inhomogeneity on the lifetime data could not fully be assessed. In principle, the discussion given by McIntosh and Sinton in Ref. [59] may be applied to assess the various impacts – but a full comprehensive consideration was beyond the scope of this work.

Since the model we chose to describe Auger recombination is fairly simple and contains few free fit parameters we apply a reverse approach to assess the validity of the model. Fig. 2a) shows the fit in comparison to the lifetime data. A good overall agreement is observed, especially considering that the data spans across multiple orders of magnitude in both carrier densities and lifetime. To estimate the uncertainty of the model the reader is referred to Fig. 2b) which shows the relative deviation of the $R_{Auger}(\Delta n)$ data normalized from the suggested model. The shaded area marks an uncertainty of ±20% and covers most measurement data – indicating this to be a reasonable upper limit uncertainty for the parameterisation. In this context, positive deviations are not necessarily problematic since they could be caused by unconsidered bulk recombination or an underestimation of surface recombination. Extrinsic limitation in our samples – be it caused by extrinsic bulk defect recombination, laterally inhomogeneous surface passivation or other effects – reduces the measured τ_{eff} and thus likely ends up causing a deviation from the τ_{Auger} model. Such limitations would be more pronounced at low injection levels due to the strong dependence of intrinsic recombination on carrier density.

A direct comparison of the proposed model to the models of Richter et al. [9] and Black and Macdonald [34] is shown in Fig. 9. It shows good overall agreement with the model by Black and Macdonald – which was to be expected since both models use the same formalism and some key assumptions are incorporated in both parameterisations. Except in the transition region defined by the different values for N_{ref} the deviation between the models is less than 5%. Comparison to the model of Richter et al. shows more severe changes. The reports of measured τ_{eff} exceeding $\tau_{Richter}$ on n-type wafers in literature indicated underestimation of intrinsic recombination in this model. However, the considerations on photon recycling in this work indicate that there actually was an *over*estimation of R_{rad} in the work of Richter, leading to the drastic differences in R_{Auger} shown in Fig. 10. This may increase the relevance of the new parameterisation for the modelling of emitter saturation currents J_{0e} even further. The grey curves for undoped silicon illustrate a fundamental difference between the work of Richter and the new models suggested by Black and Macdonald and in this work. The Coulomb screening as described by eq. (8) incorporates the assumption that a symmetric charge carrier plasma (e.g. in highly injected silicon) would also suppress Coulomb enhancement.

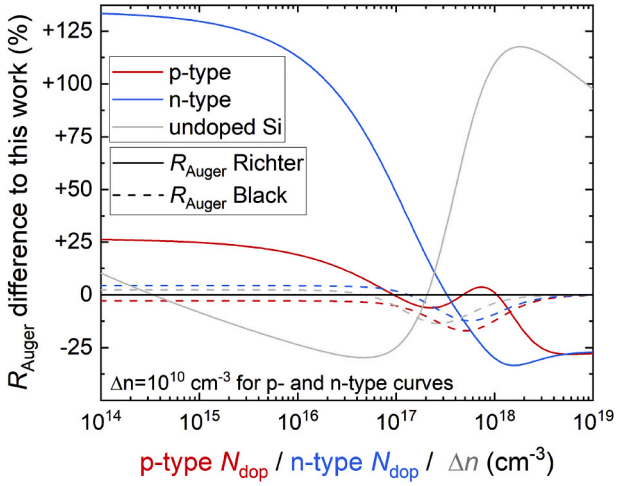

Fig. 10. Relative difference between the Auger recombination rate R_{Auger} predictions of the models by Richter et al. [9] and Black and Macdonald [34] to the model presented in this work. For p- and n-type doping $\Delta n = 10^{10}$ cm^{-3}

F. Simple Photon Recycling

As discussed above, photons emitted via radiative recombination in the silicon bulk can be reabsorbed within the wafer. This can occur via intraband absorption by free carriers – described by the fraction f_{FCA} – or via band-to-band absorption which leads to photon recycling described by the fraction f_{PR}. FCA within the wafer is insignificant for most practical cases of carrier densities below 10^{17} cm^{-3} [21,51]. The fraction f_{PR} in a sample of thickness w with planar surfaces and no additional optical features affecting the in- or outcoupling of luminescence photons can be described reasonably well with the following term:

$$f_{PR,planar\ (w,\ \Delta n)} = 0.9835 + 0.006841 \cdot \log_{10}(w) - 4.554 \cdot 10^{-9} \cdot \Delta n^{0.4612} \quad (12)$$

(w given in cm, for range 0.0001 … 0.1 cm; Δn given in cm^{-3} for $\Delta n < 10^{17}$ cm^{-3}).

The effect of total internal reflection will hence cause a strong reabsorption of emitted photons in planar samples. This case describes lifetime samples with passivated shiny-etched surfaces well and provides a good estimate for samples created from untextured silicon wafers. Since a pronounced surface texture or roughness greatly changes the angular distribution of photons after being reflected upon its first bounce, a smaller share f_{PR}

occurs for non-planar surfaces. Under the assumption that the surface texture of a sample creates a diffuse reflection the fraction f_{PR} can be described by

$$f_{PR,diffuse\ (w)} = 0.8681 - 0.0411 \cdot \log_{10}(w)^3 - 0.2393 \cdot \log_{10}(w)^2 - 0.117 \cdot \log_{10}(w) \quad (13)$$

(w given in cm, in range 0.0001 … 0.1 cm).

It should be kept in mind that these two given empirical terms describe cases with *no* or *very good* light trapping properties. Hence their usage should be accompanied by careful consideration whether a given sample should be approximated with these extreme cases.

References

[1] S.W. Glunz, F. Feldmann, SiO2 surface passivation layers – a key technology for silicon solar cells, Sol. Energy Mater. Sol. Cells 185 (2018) 260–269, https://doi.org/10.1016/j.solmat.2018.04.029.

[2] J. Schmidt, R. Peibst, R. Brendel, Surface passivation of crystalline silicon solar cells: present and future, Sol. Energy Mater. Sol. Cells 187 (2018) 39–54, https://doi.org/10.1016/j.solmat.2018.06.047.

[3] F. Haase, C. Hollemann, S. Schäfer, A. Merkle, M. Rienäcker, J. Krügener, R. Brendel, R. Peibst, Laser contact openings for local poly-Si-metal contacts enabling 26.1%-efficient POLO-IBC solar cells, Sol. Energy Mater. Sol. Cells 186 (2018) 184–193, https://doi.org/10.1016/j.solmat.2018.06.020.

[4] X. Ru, M. Qu, J. Wang, T. Ruan, M. Yang, F. Peng, W. Long, K. Zheng, H. Yan, X. Xu, 25.11% efficiency silicon heterojunction solar cell with low deposition rate intrinsic amorphous silicon buffer layers, Sol. Energy Mater. Sol. Cells 215 (2020) 110643, https://doi.org/10.1016/j.solmat.2020.110643.

[5] D. Chen, Y. Chen, Z. Wang, J. Gong, C. Liu, Y. Zou, Y. He, Y. Wang, L. Yuan, W. Lin, R. Xia, L. Yin, X. Zhang, G. Xu, Y. Yang, H. Shen, Z. Feng, P.P. Altermatt, P. J. Verlinden, 24.58% total area efficiency of screen-printed, large area industrial silicon solar cells with the tunnel oxide passivated contacts (i-TOPCon) design, Sol. Energy Mater. Sol. Cells 206 (2020) 110258, https://doi.org/10.1016/j.solmat.2019.110258.

[6] A. Richter, R. Müller, J. Benick, F. Feldmann, B. Steinhauser, C. Reichel, A. Fell, M. Bivour, M. Hermle, S.W. Glunz, Design rules for high-efficiency both-sides-contacted silicon solar cells with balanced charge carrier transport and recombination losses, Nat. Energy 6 (2021) 429–438, https://doi.org/10.1038/s41560-021-00805-w.

[7] W. Wu, J. Bao, L. Ma, C. Chen, R. Liu, Z. Qiao, J. Chen, Z. Liu, Development of industrial n-type bifacial TOPCon solar cells and modules. 36th European Photovoltaic Solar Energy Conference and Exhibition, 2019, pp. 100–102, https://doi.org/10.4229/EUPVSEC20192019-2BP.1.5.

[8] K. Yoshikawa, H. Kawasaki, W. Yoshida, T. Irie, K. Konishi, K. Nakano, T. Uto, D. Adachi, M. Kanematsu, H. Uzu, K. Yamamoto, Silicon heterojunction solar cell with interdigitated back contacts for a photoconversion efficiency over 26, Nat. Energy 2 (2017) 17032, https://doi.org/10.1038/nenergy.2017.32.

[9] A. Richter, S.W. Glunz, F. Werner, J. Schmidt, A. Cuevas, Improved quantitative description of Auger recombination in crystalline silicon, Phys. Rev. B 86 (2012) 165202, https://doi.org/10.1103/PhysRevB.86.165202.

[10] T. Niewelt, A. Richter, T.C. Kho, N.E. Grant, R.S. Bonilla, B. Steinhauser, J.-I. Polzin, F. Feldmann, M. Hermle, J.D. Murphy, S.P. Phang, W. Kwapil, M. C. Schubert, Taking monocrystalline silicon to the ultimate lifetime limit, Sol. Energy Mater. Sol. Cell. 185 (2018) 252–259, https://doi.org/10.1016/j.solmat.2018.05.040.

[11] B.A. Veith-Wolf, J. Schmidt, Unexpectedly high minority-carrier lifetimes exceeding 20msMeasured on 1 .4-?cmn- TypeSilicon wafers, Phys. Status Solidi Rapid Res. Lett. 11 (2017). https://doi.org/10.1002/pssr.201700235.

[12] F. Feldmann, M. Bivour, C. Reichel, H. Steinkemper, M. Hermle, S.W. Glunz, Tunnel oxide passivated contacts as an alternative to partial rear contacts, Sol. Energy Mater. Sol. Cells 131 (2014) 46–50, https://doi.org/10.1016/j.solmat.2014.06.015.

[13] U. Römer, R. Peibst, T. Ohrdes, B. Lim, J. Krügener, E. Bugiel, T. Wietler, R. Brendel, Recombination behavior and contact resistance of n+ and p+ poly-crystalline Si/mono-crystalline Si junctions, Sol. Energy Mater. Sol. Cells 131 (2014) 85–91, https://doi.org/10.1016/j.solmat.2014.06.003.

[14] B.A. Veith-Wolf, S. Schäfer, R. Brendel, J. Schmidt, Reassessment of intrinsic lifetime limit in n-type crystalline silicon and implication on maximum solar cell efficiency, Sol. Energy Mater. Sol. Cell. 186 (2018) 194–199, https://doi.org/10.1016/j.solmat.2018.06.029.

[15] H.T. Nguyen, S.C. Baker-Finch, D. Macdonald, Temperature dependence of the radiative recombination coefficient in crystalline silicon from spectral photoluminescence, Appl. Phys. Lett. 104 (2014) 112105, https://doi.org/10.1063/1.4869295.

[16] H. Schlangenotto, H. Maeder, W. Gerlach, Temperature dependence of the radiative recombination coefficient in silicon, Phys. Status Solidi (a) 21 (1) (1974) 357–367, https://doi.org/10.1002/pssa.2210210140.

[17] P.P. Altermatt, F. Geelhaar, T. Trupke, X. Dai, A. Neisser, E. Daub, Injection dependence of spontaneous radiative recombination in crystalline silicon: experimental verification and theoretical analysis: experimental verification and theoretical analysis, Appl. Phys. Lett. 88 (2006) 261901, https://doi.org/10.1063/1.2218041.

[18] A. Hangleiter, Coulomb enhancement of radiative and nonradiative recombination processes in semiconductors, Proc. 20th Intern. Conf. on the Physics of Semiconductors Thessaloniki (1990) 2566–2569. Greece.

[19] T. Trupke, R.A. Bardos, Self-consistent determination of the generation rate from photoconductance measurements, Appl. Phys. Lett. 85 (2004) 3611–3613, https://doi.org/10.1063/1.1807961.

[20] A. Schenk, Finite-temperature full random-phase approximation model of band gap narrowing for silicon device simulation, J. Appl. Phys. 84 (1998) 3684–3695, https://doi.org/10.1063/1.368545.

[21] A. Fell, T. Niewelt, B. Steinhauser, F.D. Heinz, M.C. Schubert, S.W. Glunz, Radiative recombination in silicon photovoltaics: modeling the influence of charge carrier densities and photon recycling, Sol. Energy Mater. Sol. Cell. 230 (2021) 111198, https://doi.org/10.1016/j.solmat.2021.111198.

[22] M.J. Kerr, A. Cuevas, General parameterization of Auger recombination in crystalline silicon, J. Appl. Phys. 91 (2002) 2473–2480, https://doi.org/10.1063/1.1432476.

[23] Hacker Hangleiter, Enhancement of band-to-band Auger recombination by electron-hole correlations, Phys. Rev. Lett. 65 (1990) 215–218, https://doi.org/10.1103/PhysRevLett.65.215.

[24] P.P. Altermatt, J. Schmidt, G. Heiser, A.G. Aberle, Assessment and parameterisation of coulomb-enhanced auger recombination coefficients in lowly injected crystalline silicon, J. Appl. Phys. 82 (1997) 4938–4944, https://doi.org/10.1063/1.366360.

[25] J. Schmidt, M. Kerr, P.P. Altermatt, Coulomb-enhanced Auger recombination in crystalline silicon at intermediate and high injection densities, J. Appl. Phys. 88 (2000) 1494–1497, https://doi.org/10.1063/1.373878.

[26] E. Yablonovitch, D.L. Allara, C.C. Chang, T. Gmitter, T.B. Bright, Unusually low surface-recombination velocity on silicon and germanium surfaces, Phys. Rev. Lett. 57 (1986) 249–252.

[27] B. Steinhauser, J.-I. Polzin, F. Feldmann, M. Hermle, S.W. Glunz, Excellent surface passivation quality on crystalline silicon using industrial-scale direct-plasma TOPCon deposition technology, Sol. RRL 142 (2018) 1800068, https://doi.org/10.1002/solr.201800068.

[28] A. Lenz, A. Huber Ip.com Disclosure Number: IPCOM000245241D.

[29] N.E. Grant, V.P. Markevich, J. Mullins, A.R. Peaker, F. Rougieux, D. Macdonald, Thermal activation and deactivation of grown-in defects limiting the lifetime of float-zone silicon, Phys. Status Solidi Rapid Res. Lett. 10 (2016) 443–447, https://doi.org/10.1002/pssr.201600080.

[30] N.E. Grant, V.P. Markevich, J. Mullins, A.R. Peaker, F. Rougieux, D. Macdonald, J. D. Murphy, Permanent annihilation of thermally activated defects which limit the lifetime of float-zone silicon, Phys. Status Solidi 213 (2016) 2844–2849, https://doi.org/10.1002/pssa.201600360.

[31] H. Höffler, F. Schindler, A. Brand, D. Herrmann, R. Eberle, R. Post, A. Kessel, J. Greulich, M.C. Schubert, Review and recent development in combining photoluminescence- and electroluminescence imaging with carrier lifetime measurements via modulated photoluminescence at variable temparatures, in: 37th EUPVSEC 2020, online.

[32] L.E. Black, D.H. Macdonald, Accounting for the dependence of coil sensitivity on sample thickness and lift-off in inductively coupled photoconductance measurements, IEEE J. Photovolt. 9 (2019) 1563–1574, https://doi.org/10.1109/JPHOTOV.2019.2942484.

[33] B. Steinhauser, T. Niewelt, A. Richter, R. Eberle, M. Schubert, Extraordinarily high minority charge carrier lifetime observed in crystalline silicon, Sol. RRL (2021), https://doi.org/10.1002/solr.202100605.

[34] L.E. Black, D.H. Macdonald, On the quantification of Auger recombination in crystalline silicon, Sol. Energy Mater. Sol. Cells 234 (2022) 111428, https://doi.org/10.1016/j.solmat.2021.111428.

[35] D.B.M. Klaassen, A unified mobility model for device simulation - II. Temperature dependence of carrier mobility and lifetime, Solid State Electron. 35 (1992) 961–967, https://doi.org/10.1016/0038-1101(92)90326-8.

[36] D.B.M. Klaassen, A unified mobility model for device simulation - I. Model equations and concentration dependence, Solid State Electron. 35 (1992) 953–959, https://doi.org/10.1016/0038-1101(92)90325-7.

[37] H. Nagel, C. Berge, A.G. Aberle, Generalized analysis of quasi-steady-state and quasi-transient measurements of carrier lifetimes in semiconductors, J. Appl. Phys. 86 (1999) 6218–6221, https://doi.org/10.1063/1.371633.

[38] B. Veith, T. Ohrdes, F. Werner, R. Brendel, P.P. Altermatt, N.-P. Harder, J. Schmidt, Injection dependence of the effective lifetime of n-type Si passivated by Al2O3: an edge effect? Sol. Energy Mater. Sol. Cells 120 (2014) 436–440, https://doi.org/10.1016/j.solmat.2013.06.049.

[39] M.J. Kerr, A. Cuevas, P. Campbell, Limiting efficiency of crystalline silicon solar cells due to Coulomb-enhanced Auger recombination, Prog. Photovoltaics Res. Appl. 11 (2003) 97–104, https://doi.org/10.1002/pip.464.

[40] J. Dziewior, W. Schmid, Auger coefficients for highly doped and highly excited silicon, Appl. Phys. Lett. 31 (1977) 346–348, https://doi.org/10.1063/1.89694.

[41] P. Jonsson, H. Bleichner, M. Isberg, E. Nordlander, The ambipolar Auger coefficient: measured temperature dependence in electron irradiated and highly

injected n-type silicon, J. Appl. Phys. 81 (1997) 2256–2262, https://doi.org/10.1063/1.364277.
[42] R. Häcker, A. Hangleiter, Intrinsic upper limits of the carrier lifetime in silicon, J. Appl. Phys. 75 (1994) 7570–7572, https://doi.org/10.1063/1.356634.
[43] N.E. Grant, T. Niewelt, N.R. Wilson, E.C. Wheeler-Jones, J. Bullock, M. Al-Amin, M. C. Schubert, A.C. van Veen, A. Javey, J.D. Murphy, Superacid-treated silicon wafers: extending the limits of bulk and surface lifetimes for high efficiency photovoltaic devices, IEEE J. Photovolt. 7 (2017) 1574–1583, https://doi.org/10.1109/jphotov.2017.2751511.
[44] T.F. Ciszek, T.H. Wang, Silicon defect and impurity studies using controlled samples, in: In: 14th EUPVSEC, Barcelona, 1997, pp. 396–399.
[45] J. Del Alamo, S. Swirhun, R.M. Swanson, Measuring and modeling minority carrier transport in heavily doped silicon, Solid State Electron. 28 (1985) 47–54, https://doi.org/10.1016/0038-1101(85)90209-6.
[46] S.E. Swirhun, Characterization of Majority and Minority Carrier Transport in Heavily Doped Silicon, Dissertation, Stanford, 1987.
[47] B. Min, H. Wagner, A. Dastgheib-Shirazi, A. Kimmerle, H. Kurz, P.P. Altermatt, Heavily doped Si:P emitters of crystalline Si solar cells: recombination due to phosphorus precipitation, Phys. Status Solidi RRL 8 (2014) 680–684, https://doi.org/10.1002/pssr.201409138.
[48] A. Kimmerle, M. Momtazur Rahman, S. Werner, S. Mack, A. Wolf, A. Richter, H. Haug, Precise parameterization of the recombination velocity at passivated phosphorus doped surfaces, J. Appl. Phys. 119 (2016) 25706, https://doi.org/10.1063/1.4939960.
[49] Di Yan, A. Cuevas, Empirical determination of the energy band gap narrowing in p + silicon heavily doped with boron, J. Appl. Phys. 116 (2014) 194505, https://doi.org/10.1063/1.4902066.
[50] S. Schäfer, R. Brendel, Accurate calculation of the absorptance enhances efficiency limit of crystalline silicon solar cells with lambertian light trapping, IEEE J. Photovolt. 8 (2018) 1156–1158, https://doi.org/10.1109/JPHOTOV.2018.2824024.
[51] A. Richter, M. Hermle, S.W. Glunz, Reassessment of the limiting efficiency for crystalline silicon solar cells, IEEE J. Photovolt. 3 (2013) 1184–1191, https://doi.org/10.1109/jphotov.2013.2270351.
[52] Andreas Fell simulations, Quokka 3.
[53] C. Schinke, P. Christian Peest, J. Schmidt, R. Brendel, K. Bothe, M.R. Vogt, I. Kröger, S. Winter, A. Schirmacher, S. Lim, H.T. Nguyen, D. Macdonald, Uncertainty analysis for the coefficient of band-to-band absorption of crystalline silicon, AIP Adv. 5 (2015) 67168, https://doi.org/10.1063/1.4923379.
[54] S.C. Baker-Finch, K.R. McIntosh, Di Yan, K.C. Fong, T.C. Kho, Near-infrared free carrier absorption in heavily doped silicon, J. Appl. Phys. 116 (2014) 63106, https://doi.org/10.1063/1.4893176.
[55] N.E. Grant, F.E. Rougieux, D. Macdonald, J. Bullock, Y. Wan, Grown-in defects limiting the bulk lifetime of p-type float-zone silicon wafers, J. Appl. Phys. 117 (2015) 55711, https://doi.org/10.1063/1.4907804.
[56] F.N. Fritsch, R.E. Carlson, Monotone piecewise cubic interpolation, SIAM J. Numer. Anal. 17 (1980) 238–246, https://doi.org/10.1137/0717021.
[57] D.E. Kane, R.M. Swanson, Measurement of the emitter saturation current by a contactless photoconductivity decay method (silicon solar cells), in: 18th IEEE Photovoltaic Specialists Conference, 1985, pp. 578–583.
[58] A.L. Blum, J.S. Swirhun, R.A. Sinton, F. Yan, S. Herasimenka, T. Roth, K. Lauer, J. Haunschild, B. Lim, K. Bothe, Z. Hameiri, B. Seipel, R. Xiong, M. Dhamrin, J. D. Murphy, Interlaboratory study of eddy-current measurement of excess-carrier recombination lifetime, IEEE J. Photovolt. 4 (2014) 525–531, https://doi.org/10.1109/jphotov.2013.2284375.
[59] K.R. McIntosh, R.A. Sinton, Uncertainty in photoconductance lifetime measurements that use an inductive-coil detector, in: In: 23rd EU PVSEC, Valencia, 2008, pp. 77–82.